BNL-108205-2015-JA

The effect of confinement on the crystalline microstructure of polymer:fullerene bulk heterojunctions

Ashraf,[a,b] D. M. N. M. Dissayanake[a] and M. D. Eisaman*[a,b,c]

[a]Sustainable Energy Technologies Department, Brookhaven National Laboratory, Upton, NY 11973, USA
[b]Department of Physics and Astronomy, Stony Brook University, Stony Brook, NY 1794, USA
[c]Department of Electrical and Computer Engineering, Stony Brook University, Stony Brook, NY 11794, USA

Accepted to Physical Chemistry Chemical Physics (PCCP)

July 2015

Sustainable Energy Technologies Department

Brookhaven National Laboratory

U.S. Department of Energy
DOE Office of Science

Notice: This manuscript has been co-authored by employees of Brookhaven Science Associates, LLC under Contract No. DE-AC02-98CH10886 with the U.S. Department of Energy. The publisher by accepting the manuscript for publication acknowledges that the United States Government retains a non-exclusive, paid-up, irrevocable, world-wide license to publish or reproduce the published form of this manuscript, or allow others to do so, for United States Government purposes.

DISCLAIMER

This report was prepared as an account of work sponsored by an agency of the United States Government. Neither the United States Government nor any agency thereof, nor any of their employees, nor any of their contractors, subcontractors, or their employees, makes any warranty, express or implied, or assumes any legal liability or responsibility for the accuracy, completeness, or any third party's use or the results of such use of any information, apparatus, product, or process disclosed, or represents that its use would not infringe privately owned rights. Reference herein to any specific commercial product, process, or service by trade name, trademark, manufacturer, or otherwise, does not necessarily constitute or imply its endorsement, recommendation, or favoring by the United States Government or any agency thereof or its contractors or subcontractors. The views and opinions of authors expressed herein do not necessarily state or reflect those of the United States Government or any agency thereof.

View Article Online
View Journal

PCCP

Accepted Manuscript

This article can be cited before page numbers have been issued, to do this please use: A. Ashraf, N. Dissanayake and M. D. Eisaman, *Phys. Chem. Chem. Phys.*, 2015, DOI: 10.1039/C5CP03399C.

This is an *Accepted Manuscript*, which has been through the Royal Society of Chemistry peer review process and has been accepted for publication.

Accepted Manuscripts are published online shortly after acceptance, before technical editing, formatting and proof reading. Using this free service, authors can make their results available to the community, in citable form, before we publish the edited article. We will replace this *Accepted Manuscript* with the edited and formatted *Advance Article* as soon as it is available.

You can find more information about *Accepted Manuscripts* in the Information for Authors.

Please note that technical editing may introduce minor changes to the text and/or graphics, which may alter content. The journal's standard Terms & Conditions and the Ethical guidelines still apply. In no event shall the Royal Society of Chemistry be held responsible for any errors or omissions in this *Accepted Manuscript* or any consequences arising from the use of any information it contains.

ROYAL SOCIETY OF CHEMISTRY

www.rsc.org/pccp

View Article Online
DOI: 10.1039/C5CP03399C

PCCP

PAPER

The effect of confinement on the crystalline microstructure of polymer:fullerene bulk heterojunctions

Received 00th January 20xx,
Accepted 00th January 20xx

DOI: 10.1039/x0xx00000x

www.rsc.org/pccp

A. Ashraf,[a,b] D. M. N. M. Dissayanake[a] and M. D. Eisaman*[a,b,c]

We investigate the effect of confinement on the coherence length and the crystalline microstructure of the polymer component of polymer:fullerene bulk heterojunction thin films using grazing incidence wide angle x-ray scattering. We find that the polymer crystallite size decreases and the alignment of the molecules along the surface normal increases, as the thin-film thickness is reduced from 920nm to < 20nm and approaches the thin-film confinement regime. Furthermore, we find that the polymer crystallite size near the surface (air interface) is lower than the crystallite size in the bulk or the bottom (substrate interface) of bulk heterojunction films thicker than the confinement regime. Variation in polymer crystallite size can cause changes in charge carrier mobility and recombination rates, which in turn affect the performance of bulk heterojunction thin film devices such as photovoltaics and photodetectors.

Introduction

The vertical confinement (film thicknesses below the typical coherence length) of a polymer:fullerene bulk heterojunction (BHJ) thin film causes a significant change in fundamental material properties compared to bulk systems.[1-4] Thin-film confinement of semi-crystalline polymers has been of great interest recently,[4-8] however the effect of confinement on the structure of the polymer within polymer:fullerene BHJ films has not been given as much attention. The addition of fullerene may have significant implications on the process of aggregation and crystallization of the polymer. Furthermore due to the vertical phase segregation of the polymer and the fullerene within a BHJ, there can be depth dependent variation of polymer crystallization which has remained unexplored in earlier studies on pure polymer systems.[9-12] Here we investigate the variation of the polymer crystallite size within a BHJ as a function of film thickness and as a function of depth within the film. This is fundamental to the understanding of the BHJ system and its application to various optoelectronic devices such as organic photovoltaics and photodetectors.[13,14] In BHJ films, within a thickness regime of 100-200 nm, the morphology has been shown to be affected by various processing conditions such as choice of solvent, drying time, thermal treatments, and the use of solvent additives.[15-17] These morphological variations directly impact the optical and electronic properties of the BHJ layer critical for device applications.[11,18] In order to direct efforts to design new polymers and thin film architectures, an in-depth understanding of BHJ microstructure and its variation due to additional complexities such as phase segregation is critical.

The present work focuses on using grazing incidence wide angle X-ray scattering (GIWAXS) to probe the structure of a poly[3-hexylthiophene-2,5-diyl] (P3HT) and [6,6]-phenyl C61 butyric acid methyl ester (PCBM) BHJ layer. We find that as the thickness of the BHJ is decreased to the ultrathin regime of < 20nm, surface-energy effects at the interfaces and kinetics of film formation play an increasingly important role in determining the BHJ microstructure. Additionally, we probe variation with depth within a film by employing surface-sensitive GIWAXS (angle of incidence = 0.07˚ < the critical angle of 0.1˚, yielding a depth sensitivity of ~11nm) on as-cast BHJ films as well as BHJ films that have been inverted onto a new substrate exposing the buried interface of the film. These results allow us to directly measure the variation in microstructure at the interfaces (air/film, film/substrate) and compare them to the bulk.

The polymer in BHJ films crystallizes with a lamellar alignment parallel to the substrate with the side-chain groups perpendicular to the substrate. In the conventional crystallographic notation this lamellar direction is defined as <100>.[14] We use the term "crystallite" to refer to a set of π-stacked conjugated polymer segments that participate in lamellar stacking and result in diffraction peaks in the grazing incidence geometry. The coherence length as determined using the FWHM of the <100> scattering peak is identified as the "crystallite size" in this direction. Although several studies

[a.] Sustainable Energy Technologies Department, Brookhaven National Laboratory, Upton, NY, 11973, USA.
[b.] Department of Physics and Astronomy, Stony Brook University, Stony Brook, NY, 11794, USA.
[c.] Department of Electrical and Computer Engineering, Stony Brook University, Stony Brook, NY, 11794, USA.

Published on 01 July 2015. Downloaded by BNL Research Library on 01/07/2015 16:33:19.

Physical Chemistry Chemical Physics Accepted Manuscript

View Article Online
DOI: 10.1039/C5CP03399C

Published on 01 July 2015. Downloaded by BNL Research Library on 01/07/2015 16:33:19.

have tried to quantify the extent of disorder in polymers in various ways,[7,19-21] in this manuscript we use the FWHM of the normalized scattering intensity as a function of the polar angle χ with respect to the surface normal at the q-vector of the <100> peak, as a measure of the extent of alignment of the polymer molecules (molecular packing order) along the surface normal.

Using spin-cast BHJ films (thicknesses ranging from 15nm – 920nm) on poly(3,4-ethylenedioxythiophene) poly(styrenesulfonate) (PEDOT-PSS), we find that the polymer crystallite size in the bulk of the film increases from 6.86 (+/- 0.04) nm to 21.49 (+/- 0.19) nm as the film thickness increases from 15nm to 920nm, with the asymptotic crystallite size of ~21nm occurring for film thicknesses $\geq$ 200nm. The molecular packing order, as defined above, decreases as the film thickness is increased. Additionally, we find that the crystallite size on the surface of a BHJ film thicknesses >100nm is reduced compared to the crystallite size at the buried interface between the BHJ and the PEDOT-PSS.

Experimental

Sample Preparation

Poly(3-hexylthiophene) (P3HT) was obtained from Rieke Metal Inc. (4002-EE, Lot # BS21-21) with a molecular weight, Mw of 40,000 – 60,000 Daltons and regioregularity, RR of 90-94%. [6,6]-Phenyl-C-61-butyric acid methyl ester (PCBM) of purity greater than 99.5% was obtained from American Dye Source Inc. (ADS61BFA, Lot # 12E011E). The substrates used were microscope slide glass obtained from Thermo Fisher Scientific, and silicon wafers with a native silicon dioxide layer and also 300nm silicon dioxide on silicon wafers obtained from Ted Pella Inc. The substrates were cleaned by sonication for 15 minutes in acetone, then 15 minutes in isopropanol, and finally 15 minutes in deionized water. The cleaned substrates were dried using N_2 gas and exposed to UV ozone for 300s. P3HT and PCBM solutions were prepared in 1:1, 2:1, and 1:2 ratios using 1,2-dichlorobenzene (anhydrous, 99%), Sigma Aldrich, St. Louis, MO. The solutions were prepared inside a glove box (O2 < 0.1ppm, H2O < 0.1ppm) and stirred for 2 hours at 50°C using a Teflon coated magnetic stirrer. After stirring they were filtered through a PTFE syringe filter with a pore size of 0.45µm and transferred into a fresh vial. Total solids solutions were prepared with concentrations of 2mg/ml, 5mg/ml 10mg/ml, 20mg/ml and 50mg/ml. These were pipetted onto the substrate and spun at 700rpm for 40s inside the glove box. After the films were dry (judging by the drastic visual change in coloration of the film), they were thermally treated at 150°C for 10 minutes inside the glovebox.

Grazing-incidence wide-angle X-ray scattering

GIWAXS measurements were performed at the undulator-based X9 endstation at the National Synchrotron Light Source (NSLS), Brookhaven National Laboratory. Two-dimensional scattering images were acquired using a flat area detector, positioned 280mm from the sample, and using an X-ray wavelength of 0.918nm (photon energy of 13.5keV). Raw data conversion to q-space was accomplished by measuring a standard sample with known scattering features (Silver Behenate), and accounting for detector position and tilt angle in the grazing incidence geometry. The incident beam was collimated using slits and focused onto the sample position using a KB mirror system; the beam size at the sample position was approximately 200µm horizontal width and 50µm vertical width. Measurements were performed at a variety of incident angles (0.07˚, 0.10˚, 0.12˚, 0.15˚, and 0.20˚); all measurements above the critical angle (0.1˚ degrees for P3HT) had similar features. The results presented in the manuscript representing the bulk of the film use the data at 0.20˚, which is well above the critical angle for any of the films studied, and is thus representative of the entire film.

Results and Discussion

The polymer in BHJ films crystallizes with a strong degree of lamellar alignment parallel to the substrate with the side groups perpendicular to the substrate ("edge on", as shown in Fig. 1). We define q_z as the component of the scattering vector, q, perpendicular to the sample surface, while $q_{x,y}$ is defined along the sample surface. The 2D GIWAXS pattern in Fig. 1 shows three peaks <h00> in the substrate-normal (q_z) direction. Extracting a line cut in this direction allows us to calculate the spacing between the P3HT lamellae in the substrate-normal direction. For a film with a thickness of 92nm we measure a layer spacing of 1.7nm, which is consistent with previous reports.[12-14,17] We have computed the P3HT crystallite size from the <100> scattering peak-width using a Scherrer analysis, accounting for instrumental broadening of the peak and intersection of the scattering with the detector geometry.[22] Instrument details can be found in the experimental section. For a film with a thickness of 92nm we obtain a polymer crystallite size of 19.8nm, which agrees with polymer crystallite size in BHJ films from previous reports.[12-14,17]

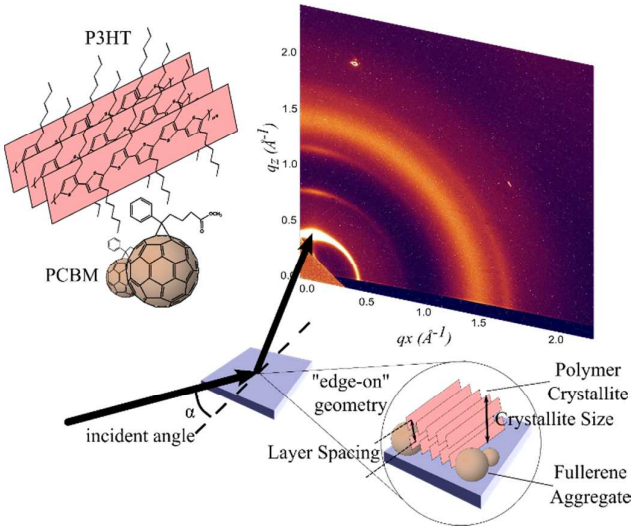

Fig. 1 Schematic of the GIWAXS measurement geometry. The polymer chains are shown to form a crystallite in the edge-on orientation. In this alignment the P3HT back-

Physical Chemistry Chemical Physics Accepted Manuscript

This journal is © The Royal Society of Chemistry 2015

View Article Online
DOI: 10.1039/C5CP03399C

Published on 01 July 2015. Downloaded by BNL Research Library on 01/07/2015 16:33:19.

bone is oriented parallel to the substrate, and the side chains pointing in the substrate-normal direction.

BHJ films of different thicknesses (ranging from 15nm – 920nm) were spun on PEDOT-PSS/Glass substrates. The thicknesses were determined using variable angle spectroscopic ellipsometry, the details for which can be found in previous reports.[11] Fig. 2 shows the P3HT crystallite size as well as the layer spacing in the substrate-normal direction between the P3HT lamellae. We find that as the thickness of the active layer is reduced, the crystallite size of the polymer decreases. In the ultrathin film of 15nm, we find that the crystallite size decreases to 6.9nm as a combination of confinement and enhanced solvent evaporation frustrate the crystallization process and produce smaller P3HT crystallites. For films of thickness >100nm, the crystallite size approaches ~21nm as an asymptotic limit. In order to confirm crystallite size saturation, a thick film of 920nm is also measured for which the polymer crystallite size does not change significantly. Furthermore, using a line cut along $q_{x,y}$ to calculate the isotropic crystallite size for films thicker than 200nm, we have verified that no significant variation can be seen in the crystallite size due to P3HT orientation. The molecular layer spacing within the polymer in the substrate-normal direction was also measured and is shown in Fig. 2. Although there are small variations (<1Å) as the thickness of the BHJ is increased, the molecular layer spacing remains at ~1.7nm.

Additionally a peak at <010> is also visible representing the π-π stacking direction. Crystallite sizes in this direction are calculated to be ~4nm and the π-π stacking distance ~0.4nm consistent with previous reports.[17]

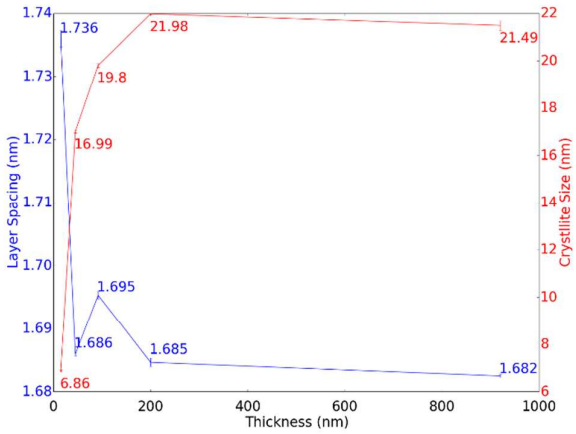

Fig. 2 Polymer crystallite size (red, right) extracted using the Scherrer analysis as discussed in the text and layer spacing between polymer molecules in the surface normal direction (blue, left) for BHJ films of various thicknesses. The error bars represent the standard deviation from multiple spots on the film. Solid lines are to guide the eye.

The P3HT in BHJ thin films shows a strong preference for "edge-on" orientation. In this alignment the P3HT back-bone is oriented parallel to the substrate, with the backbones stacked in the substrate-normal direction and the P3HT side chains pointing in the substrate-normal direction.[13,23,24] This most likely arises from surface effects at the substrate/BHJ and the BHJ/air interface, where the P3HT side-chains preferentially interact with these interfaces to lower overall surface energy. This effect of interface alignment has been shown previously in liquid crystals and decays exponentially from the interface towards the bulk.[25] As the thickness of the BHJ film is reduced, the substrate/BHJ and the BHJ/air interfaces are brought closer together therefore further aligning the P3HT molecules. The normalized scattering intensity as a function of the polar angle χ, with respect to the surface normal at the q-vector of the <100> peak, gives us a measure for the P3HT orientation. Fig. 3(a) shows that the lamellar alignment is predominantly parallel to the substrate (i.e., edge-on alignment) at $\chi \sim 0$. The inset in Fig. 3(b) shows the normalized scattering intensities for different film thicknesses as function of χ around $\chi \sim 0$. Fitting the intensity to a Gaussian profile gives us the FWHM, which is used as a measure of the extent of P3HT alignment. Fig. 3(b) shows that as the film thickness is reduced from a BHJ film of >100nm to the thin-film confinement regime, the FWHM decreases indicating that the P3HT molecules become further aligned in the edge-on direction. This agrees well with previous works where P3HT crystallites have been seen to become more ordered as the thickness of a BHJ film is reduced.[11]

Physical Chemistry Chemical Physics Accepted Manuscript

View Article Online
DOI: 10.1039/C5CP03399C

Published on 01 July 2015. Downloaded by BNL Research Library on 01/07/2015 16:33:19.

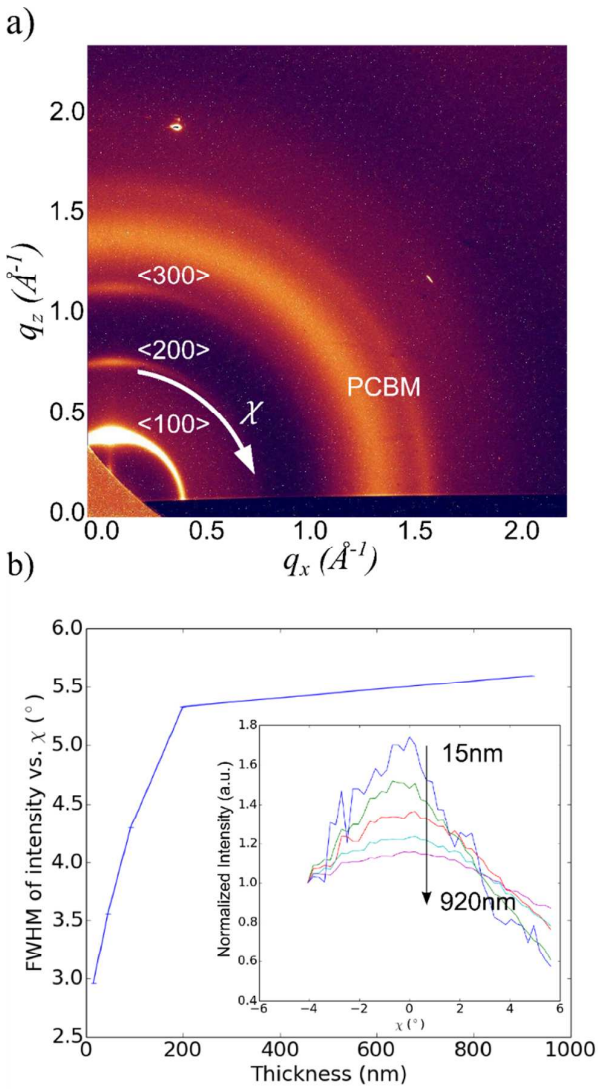

Fig. 3 (a) Two-dimensional scattering image for polymer:fullerene BHJ thin film showing polymer lamellar alignment parallel to the substrate ("edge on") as demonstrated by the <h00> scattering peaks, and a characteristic diffuse PCBM scattering ring. Also shown is the direction of the polar angle χ. (b) The full width at half maximum (FWHM) of the normalized intensity vs. χ at the <100> peak position for films of different thicknesses. Inset shows the normalized intensity (a.u.) vs. χ for films of different thicknesses.

Surface energy effects at the interfaces of a BHJ film have also been shown to cause a linear concentration gradient of the polymer in a polymer:fullerene blend film in the substrate-normal direction.[9,11,26,27] It has been seen in blend films that an interfacial layer of high polymer concentration is formed at the BHJ/air interface and an interfacial layer of higher fullerene concentration is formed at the substrate/BHJ interface.

The inset in Fig. 4 shows the change in the crystallite size for films of different thicknesses in the top, bulk and the bottom of the film. The top of the film is probed using a surface sensitive GIWAXS angle of 0.07˚ (critical angle for this film ~ 0.1˚). For a BHJ film, this gives a depth sensitivity of 11.6nm from the air interface. The sample is then immersed in a water bath to dissolve the PEDOT-PSS and float the BHJ film. A clean substrate is then used to recover the BHJ film but inverted from its initial state. This film is dried by flowing nitrogen and then left in vacuum overnight. Scattering data collected at a grazing incidence angle of 0.07˚ on this film then gives us information from the bottom 11.6nm of the original BHJ film, the part of the film that was previously adjacent to the PEDOT:PSS layer. It is important to point out that for a 15nm thick film, the regions to which we are sensitive in the original and inverted films overlap in the middle ~9nm. Therefore scattering data on this film serves as a check to validate that the process of the inversion does not affect the GIWAXS measurement results. The inset in Fig. 4 also shows the bulk crystallite size calculated using a 0.2˚ incident angle as a reference.

We find that in the top 11.6nm of the BHJ film near the air interface, the crystallite sizes are smaller than at the PEDOT:PSS interface or in the bulk. This is true for films of thickness ≥ 92nm. For the ultrathin films, the crystallite size at the air interface ≈ crystallite size at the PEDOT:PSS interface. This confirms that the inversion process does not affect the results. Fig. 4 shows the change of crystallite size (Δ Crystallite size) from the bottom 11.6nm (PEDOT:PSS interface) to the top 11.6nm (air interface). For the ultrathin films the variation is ~ 0nm as we are probing roughly the same volume in both cases. However for the films with thickness ≥100nm, we measure a decrease of about 5-7nm in the crystallite size between the bottom (PEDOT:PSS interface) and the top (air interface) of the film.

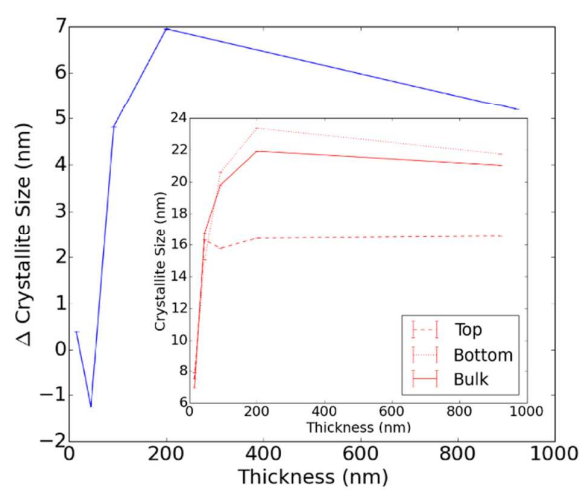

Fig. 4 The difference in the polymer crystallite size (Δ Crystallite size (nm)) between the bottom (~11nm) and the top (~11nm) of the BHJ film as a function of film thickness. The inset shows the calculated polymer crystallite sizes in the top (surface sensitive GIWAXS on the as-cast film), bottom (surface sensitive GIWAXS on a film that was physically inverted from its original state), and the bulk (GIWAXS at an incidence angle well above the critical angle) of the BHJ film.

Although this variation in crystallite size within the depth of the film could naively be attributed to the variation in PCBM concentration due to phase segregation, in order to understand the effect of a PCBM concentration gradient on the polymer crystallite size, we measure the bulk polymer crystallite size using GIWAXS from samples of different blend

Physical Chemistry Chemical Physics Accepted Manuscript

This journal is © The Royal Society of Chemistry 2015

View Article Online
DOI: 10.1039/C5CP03399C
PCCP Paper

Published on 01 July 2015. Downloaded by BNL Research Library on 01/07/2015 16:33:19.

ratios but of the same concentration. Blend ratios are chosen such that the polymer volume fraction is similar at the air interface, bulk, and the PEDOT:PSS interface in a phase segregated film of thickness >100nm.[11] For BHJ films with P3HT:PCBM ratios of 1:2, 1:1, and 2:1, we calculate a bulk crystallite size of 19.5nm, 21nm, 17.5nm respectively. The bulk crystallite size of the polymer in a BHJ film does not vary significantly with polymer fraction (in the range of polymer fraction variation that can be seen within a phase segregated film).

Therefore, the observed variation of crystallite size within the film depth cannot be due to the change in the PCBM fraction, but can likely be attributed to the variation in the kinetics of film formation. The Avrami equation can be adopted as a rough model to understand the kinetics of crystallization within BHJ films.[28] The Avrami expression has been used previously to model the extent of phase-volume development as a function of time.[12] In our case, the films are in a steady state after the process of crystallization has already been completed. However there is a variation of the extent of phase development as a function of the depth of the film due to the time it takes for the solvent to escape from different sections in the film. Therefore we develop an Avrami expression where the phase development of crystallization, α, is written as a function of the distance from the air interface, x, within a BHJ film:

$$\alpha(x) = 1 - e^{Kx^n}, \quad (1)$$

where K is the rate constant and n is the Avrami exponent. To quantify the extent of polymer crystallization, α, we use the integrated intensity of the <100> peak over q_z normalized by the maximum intensity value.[12]

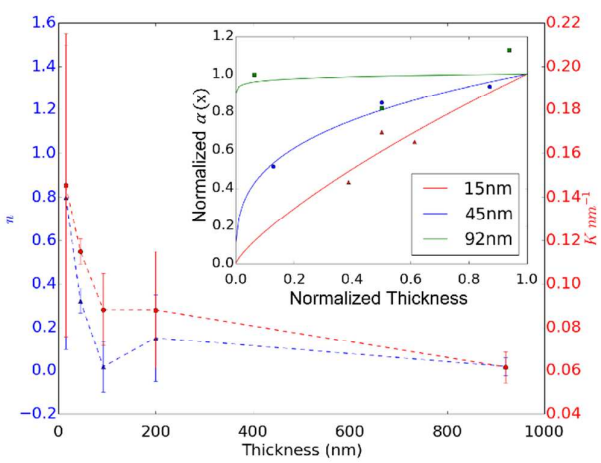

Fig. 5 The Avrami exponent n (blue, left) and the rate constant K (nm^{-1}) (red, right) calculated for BHJ films of several different thicknesses. The dotted lines are guide to the eye. The error bars are calculated using the covariance matrix from the least squares fitting of the data to Eq. (1). The inset shows normalized α(x) as a function of the normalized depth for BHJ films of three difference thicknesses (15nm, 45nm, and 92nm). The solid lines represent the best fit curves.

For each film, we calculate α for three points in the depth of the film: the top 11.6nm, the bulk that is used as the center value, and the bottom 11.6nm. The calculated Avrami exponent (n) and the rate constant (K) for BHJ films of different thicknesses are shown in Fig. 5. The error bars are calculated using the covariance matrix from the least squares fitting of the data to Eq. (1). The inset in Fig. 5 shows α(x) as a function of the normalized depth for BHJ films of three difference thicknesses (15nm, 45nm, and 92nm). The solid lines represent the normalized best fit curves to Eq. (1). The rate constant for films in the thin-film confinement regime is higher than films of larger thicknesses, suggesting that the crystallization in the thinner films is more rapid as a function of depth. In films of larger thicknesses, the rate of crystallization is lower as there is more volume further away from the air interface, from which the solvent has to escape. The Avrami exponent n has contributions from both nucleation and growth mechanism and can be written as $n = n_I + n_G$, where n_I relates to the nucleation and the n_G to the growth mechanism.[28] The nucleation factor, n_I, is expected to have values between 1, which refers to constant nucleation, and 0, which refers to quenched-in nuclei. Assuming that the growth-mechanism for films of all thicknesses is the same, we can then understand the change in the Avrami exponent as a function of thickness shown in Fig. 5 as change in the nucleation rate. For films in the thin-film confinement regime we get a value for the Avrami exponent to be close to 1 indicating constant nucleation. As the thickness of the BHJ film is increased, we approach a value of ~0.05 which can be explained by the quenching of the nucleation of polymer crystallization.

This rough model for polymer crystallization fits the data well and provides a likely explanation for the depth-dependence of polymer crystallization in a BHJ film. In an electronic device, the top of the film forms the interface to a metal contact that plays a crucial role in band alignment and recombination dynamics. The variation in crystallite size is particularly important as it changes the interfacial area between donor and acceptor materials. As excitons are dissociated at these interfaces, crystallite size variation significantly affects the charge transport and pathways for charge percolation. This in turn can cause changes in mobility and recombination, and therefore determine the performance of an electronic device.[29-34]

Conclusions

The confinement of polymer:fullerene BHJ films significantly alters the structural and crystallographic properties of the polymer. We presented a crystallographic analysis of polymer:fullerene thin films of different thicknesses using GIWAXS, and determined that the crystallite size of the polymer in BHJs decreases and the molecular alignment of the polymer along the surface normal increases in the thin-film confinement regime. Furthermore, we studied the change in the crystallite size of the polymer within the depth of the film for different film thicknesses. We found that for thicknesses ≥100nm, the crystallite size on the top ~11nm of the film is reduced compared to the crystallite size in the bottom and the bulk of the film. We provided a likely explanation for this by using the Avrami equation to model the kinetics of film

Physical Chemistry Chemical Physics Accepted Manuscript

View Article Online
DOI: 10.1039/C5CP03399C

formation. These results shed new light on the physics of bulk-heterojunction film formation, enabling material optimization and design for applications such as bulk heterojunction organic photovoltaics.

Acknowledgements

Research was carried out in part at the Center for Functional Nanomaterials, Brookhaven National Laboratory, which is supported by the U.S. Department of Energy, Office of Basic Energy Sciences, under Contract No. DE-AC02-98CH10886. Use of the National Synchrotron Light Source, Brookhaven National Laboratory, was supported by the U.S. Department of Energy, Office of Science, Office of Basic Energy Sciences, under Contract No. DE-AC02-98CH10886. This work was also partially supported by the U. S. Department of Energy, Sustainable Energy Technologies Department under contract DE-AC02-98CH10886. We thank Kevin Yager and Ben Ocko for useful discussions.

Notes and References

1 C. L. Soles, E. K. Lin, J. L. Lenhart, R. L. Jones, W. Wu, D. L. Goldfarb, and M. Angelopoulos, *Journal of Vacuum Science & Technology B: Microelectronics and Nanometer Structures*, 2001, **19**, 2690.
2 C. L. Soles, J. F. Douglas, W. Wu, and R. M. Dimeo, *Macromolecules*, 2003, **36**, 373.
3 D. L. Goldfarb, M. Angelopoulos, E. K. Lin, R. L. Jones, C. L. Soles, J. L. Lenhart, and W. Wu, *Journal of Vacuum Science & Technology B: Microelectronics and Nanometer Structures*, 2001, **19**, 2699.
4 S. Joshi, S. Grigorian, U. Pietsch, P. Pingel, A. Zen, D. Neher, and U. Scherf, *Macromolecules*, 2008, **41**, 6800.
5 S. Himmelberger, J. Dacuña, J. Rivnay, L. H. Jimison, T. McCarthy-Ward, M. Heeney, I. McCulloch, M. F. Toney, and A. Salleo, *Adv. Funct. Mater.*, 2012, **23**, 2091.
6 D. T. Duong, M. F. Toney, and A. Salleo, *Phys. Rev. B*, 2012, **86**, 205205.
7 L. H. Jimison, S. Himmelberger, D.T. Duong, J. Rivnay, M. F. Toney, and A. Salleo, *J. Polym. Sci. B Polym. Phys.,* 2013, **51**, 611.
8 S. C. B. Mannsfeld, A. Virkar, C. Reese, M. F. Toney, and Z. Bao, *Advanced Materials*, 2009, **21**, 2294.
9 M. Campoy-Quiles, T. Ferenczi, T. Agostinelli, P. G. Etchegoin, Y. Kim, T. D. Anthopoulos, P. N. Stavrinou, D. D.C. Bradley, J. Nelson, *Nature Materials*, 2008, **7**, 158.
10 S. Engmann, V. Turkovic, P. Denner, H. Hoppe, and G. Gobsch, *Journal of Polymer Science Part B: Polymer Physics*, 2012, **50**, 1363.
11 A. Ashraf, D. M. N. M. Dissanayake, D. S. Germack, C. Weiland, and M. D. Eisaman, *ACS Nano*, 2014, **8**, 323.
12 W. Wu, U. Jeng, C. Su, K. Wei, M. Su, M. Chiu, C. Chen, W. Su, C. Su, and A. Su, *ACS Nano*, 2011, **5**, 6233.
13 R. J. Kline, M. D. McGehee, and M. F. Toney, *Nature Materials*, 2006, **5**, 222.
14 P. Peumans, A. Yakimov, and S. R. Forrest, *Journal of Applied Physics*, 2003, **93**, 3693.
15 J. Huang, Y. Yao, T. Moriarty, K. Emery, G. Li, V. Shrotriya, and Y. Yang, *Nature Materials*, 2005, **4**, 864.
16 R. Stalder, C. Grand, J. Subbiah, F. So, and J. R. Reynolds, *Polymer Chemistry*, 2011, **3**, 89.
17 W. Chen, M. P. Nikiforov, and S. B. Darling, *Energy & Environmental Science*, 2012, **5**, 8045.
18 D. M. N. M. Dissanayake, A. Ashraf, Y. Pang, and M. D. Eisaman, *Adv. Energy Mater.*, 2014, **4**, 1300525.
19 M. Brinkmann, and P. Rannou, *Adv. Funct. Mater.,* 2007, **17**, 101.
20 I. M. Craig, C. T. Tassone, S. H. Tolbert, and B. J. Schwartz, *The Journal of Chemical Physics*, 2010, **133**, 044901.
21 S. Lilliu, T. Agostinelli, E. Pires, M. Hampton, J. Nelson, and J. E. Macdonald, *Macromolecules*, 2011, **44**, 2725.
22 D. M. Smilgies, *J Appl. Cryst.*, 2009, **42**, 1030.
23 H. Yang, T. J. Shin, L. Yang, K. Cho, C. Y. Ryu, and Z. Bao, *Adv. Funct. Mater.*, 2005, **15**, 671.
24 H. Sirringhaus, P. J. Brown, R. H. Friend, M. M. Nielsen, K. Bechgaard, B. M. W. Langeveld-Voss, A. J. H. Spiering, R. A. J. Janssen, E. W. Meijer, and P. Herwig, Nature, 1999, **401**, 685.
25 P. J. Gennes, *The Physics of Liquid Crystals (International Series of Monographs on Physics)*, *2nd ed.* Oxford University Press: New York, 1993 Vol. 10.
26 D. S. Germack, C. K. Chan, R. J. Kline, D. A. Fischer, D. J. Gundlach, M. F. Toney, L. J. Richter, and D. M. DeLongchamp, *Macromolecules*, 2010, **43**, 3828.
27 P. G. Karagiannidis, D. Georgiou, C. Pitsalidis, A. Laskarakis, and S. Logothetidis, *Materials Chemistry and Physics*, 2011, **129**, 1207.
28 P. Bruna, D. Crespo, R. Gonzalez-Cinca, and E. Pineda, *Journal of Applied Physics*, 2006, **100**, 054907.
29 R. C. Nieuwendaal, H. W. Ro, D. S. Germack, R. J. Kline, M. F. Toney, C. K. Chan, A. Agrawal, D. Gundlach, D. L. VanderHart, and D. M. Delongchamp, *Adv. Funct. Mater.*, 2012, **22**, 1255.
30 U. Zhokhavets, T. Erb, G. Gobsch, M. Al-Ibrahim, and O. Ambacher, *Chemical Physics Letters*, 2006, **418**, 347.
31 D. H. Kim, Y. D. Park, Y. Jang, H. Yang, Y. H. Kim, J. I. Han, D. G. Moon, S. Park, T. Chang, and C. Chang, *Adv. Funct. Mater.*, 2005, **15**, 77.
32 M. Chiu, U. Jeng, C. Su, K. S. Liang, and K. Wei, *Adv. Mater.*, 2008, **20**, 2573.
33 C. Liu, M. Su, J. Jiang, Y. Su, C. Su, C. Chen, C. Tsao, and K. Wei, *ACS Appl. Mater. Interfaces,* 2013, **5,** 5413.
34 M. T. Dang, L. Hirsch, G. Wantz, and J. D. Wuest, Chem. Rev., 2013, **113**, 3734.

Published on 01 July 2015. Downloaded by BNL Research Library on 01/07/2015 16:33:19.
Physical Chemistry Chemical Physics Accepted Manuscript

This journal is © The Royal Society of Chemistry 2015